World Academy of Science, Engineering and Technology
International Journal of Mechanical and Mechatronics Engineering
Vol:9, No:12, 2015

Finite Element Method Analysis of Occluded-Ear Simulator and Natural Human Ear Canal

M. Sasajima, T. Yamaguchi, Y. Hu, Y. Koike

***Abstract*—**In this paper, we discuss the propagation of sound in the narrow pathways of an occluded-ear simulator typically used for the measurement of insert-type earphones. The simulator has a standardized frequency response conforming to the international standard (IEC60318-4). In narrow pathways, the speed and phase of sound waves are modified by viscous air damping. In our previous paper, we proposed a new finite element method (FEM) to consider the effects of air viscosity in this type of audio equipment. In this study, we will compare the results from the ear simulator FEM model, and those from a three dimensional human ear canal FEM model made from computed tomography images, with the measured frequency response data from the ear canals of 18 people.

***Keywords*—**Ear simulator, FEM, viscosity, human ear canal.

I. Introduction

An occluded-ear simulator is a piece of equipment designed to simulate the acoustic properties of the ear canal and eardrum of a typical human ear, and can be used to measure the frequency response of insert-type earphones. A typical equipment setup to measure the frequency response of an earphone is shown in Fig. 1. To accurately measure the characteristics of any earphone, it is necessary to use such a standardized simulator. The occluded-ear simulator modeled in this study conforms to the international standard, IEC60318-4: Occluded-ear simulator for the measurement of earphones coupled to the ear by means of ear inserts [1]. This type of ear simulator has very narrow pathways to control the acoustic resistance. Conventional acoustic analysis is used predominantly for relatively large structures and equipment. There are very few methods for analyzing the acoustic properties of equipment with a small volume, such as an occluded-ear simulator. In narrow sound pathways, the speed and phase of the sound waves are modified by viscous air damping. Therefore, to accurately analyze the acoustic properties of a small ear simulator, the effect of air viscosity should be considered, which is not typically done in conventional acoustic analysis. We have proposed a new finite element method (FEM) that considers the effects of air viscosity on sound in narrow pathways [2], [3]. This method was developed as an extension of the acoustic FEMs proposed by Biot [4], [5] and Yamaguchi [6]–[9] for porous, sound-absorbing materials. We attempted a numerical analysis in the frequency domain using our acoustic solver, which utilizes the proposed FEM to model an occluded-ear simulator with narrow pathways.

M. Sasajima, Y. Hu and Y. Koike are with the Strategic Research & Development Division, Foster Electric Co. Ltd., 196-8550, 1-1-109 Tsutsujigaoka, Akishima, Tokyo, Japan (Phone: 042-847-3334; e-mail: sasajima@foster.co.jp, fhuy@foster.co.jp, koike@foster.co.jp).

T. Yamaguchi is with the Department of Mechanical Science and Technology, Faculty of Science and Technology, Gunma University, 376-8515, 1-5-1, Tenjin-cho, Kiryu, Gunma, Japan (e-mail: yamagme3@gunma-u.ac.jp).

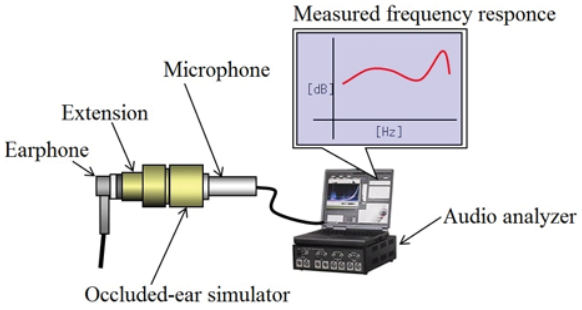

Fig. 1 Typical equipment setup to measure the frequency response of an insert-type earphone using an occluded-ear simulator

A 3D human ear canal model was constructed using Digital Image and Communication in Medicine (DICOM) data produced by a computed tomography (CT) system (GE Medical Systems, LightSpeed VCT). The image data was 0.625 mm pitch slices of a human body with interpolation data at the mid-point of 0.315 mm. The 3D modeling software OsiriX was utilized to construct a stereolithographic model of triangle surface elements as shown in Fig. 2. Finally, a 3D tetrahedral solid mesh model was constructed using the HyperMesh meshing software.

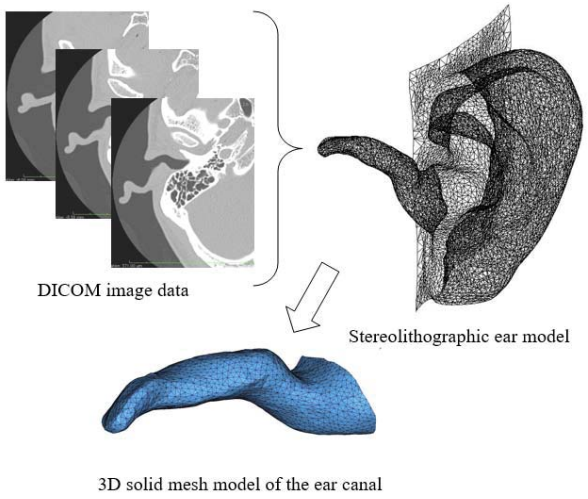

Fig. 2 DICOM image data, stereolithographic human ear model, and 3D solid mesh model

We can therefore compare the results obtained from FEM modeling of an occluded-ear simulator and a human ear canal, with actual measurements from human ears.

II. Numerical Procedures

We developed a new FEM that incorporates the air viscosity at small amplitudes. Fig. 3 shows the Cartesian coordinate system for a tetrahedron element, showing the nodes, and constant strain elements. Here, u_x, u_y, and u_z are the displacements in the x, y, and z directions, respectively, at arbitrary points in the element.

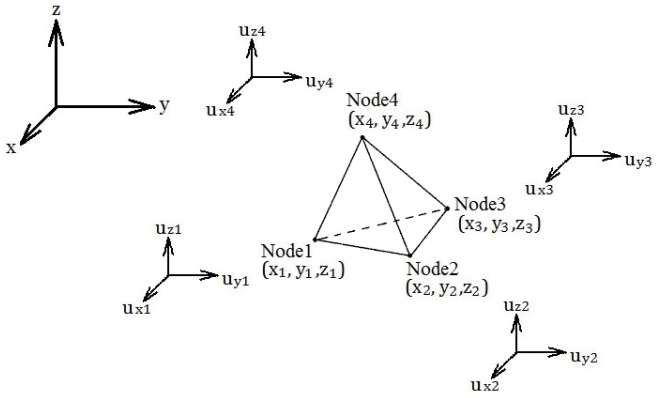

Fig. 3 Cartesian coordinate system and constant strain elements

In this case, the strain energy $\tilde{U}$ is expressed as

$$\tilde{U} = \frac{1}{2} E \iiint_e \left(\frac{\partial u_x}{\partial x} + \frac{\partial u_y}{\partial y} + \frac{\partial u_z}{\partial z} \right)^2 dxdydz \quad (1)$$

where E is the bulk modulus of the air elasticity and u is the time derivative of the particle displacement. Therefore, the kinetic energy $\tilde{T}$ is expressed as

$$\tilde{T} = \frac{1}{2} \iiint_e \rho \{\dot{u}\}^T \{\dot{u}\} dxdydz \quad (2)$$

where ρ is the effective density of the element and T represents a transposition. The viscosity energy $\tilde{D}$ of a viscous fluid is expressed as

$$\tilde{D} = \iiint_e \frac{1}{2} \{\bar{T}\}^T \{\Gamma\} dxdydz \quad (3)$$

where $\{\bar{T}\}$ is the stress vector attributable to the viscosity and $\{\Gamma\}$ is the strain vector. We then considered the formulation of a motion equation of an element in order to consider the viscous damping in an acoustic analysis model.

The total energy $\tilde{E}$ is derived using

$$\tilde{E} = \tilde{U} + \tilde{D} - \tilde{T} - \tilde{V} \quad (4)$$

where $\tilde{V}$ is the potential energy. Using Lagrange's equations, we obtain the following discretized equation for an element:

$$\frac{d}{dt} \frac{\partial \tilde{T}}{\partial \dot{u}_{ei}} - \frac{\partial \tilde{T}}{\partial u_{ei}} + \frac{\partial \tilde{U}}{\partial u_{ei}} - \frac{\partial \tilde{V}}{\partial u_{ei}} + \frac{\partial \tilde{D}}{\partial u_{ei}} = 0 \quad (5)$$

where u_{ei} is the i^{th} component of the nodal displacement vector $\{u_e\}$ and $\dot{u}_{ei}$ is the i^{th} component of the nodal particle velocity vector $\{\dot{u}_e\}$. We obtain the following discretized equation of an element by substituting (1)–(3) into (5):

$$-\omega^2 [M_e]\{u_e\} + [K_e]\{u_e\} + j\omega [C_e]\{u_e\} = \{f_e\} \quad (6)$$

Here, we use $\{\dot{u}_e\} = j\omega\{u_e\}$ because a periodic motion with angular frequency ω is assumed. $[M_e]$, $[K_e]$, $[C_e]$ and $\{f_e\}$ are the element mass matrix, element stiffness matrix, element viscosity matrix, and nodal force vector, respectively. All nodal particle displacements can be calculated by solving (6). In addition, the strain and sound pressure of all elements can be calculated from the nodal particle displacements.

III. Calculation

A. Damping Analysis of an Occluded-Ear Simulator Using the Proposed 3D FEM

First, we conducted an acoustic damping analysis of the ear simulator. As shown in Fig. 4, we use a half model due to symmetry about the center plane, with a height of 14.0 mm and a main cavity radius of 7.5 mm. Narrow pathways from the main cavity lead to two Helmholtz resonance cavities at heights of 0.69 and 0.17 mm. Viscous air damping occurs in these narrow pathways. The volume and size of the two half ring resonators are such that resonance occurs at 1,800 Hz and 5,000 Hz. The model uses first order tetrahedral elements each with four nodes. The calculations were performed with a total of 161,928 elements and 37,170 nodes. The narrow pathways were divided into seven elements in the vertical direction. We assumed the effective density $\rho_0 = 1.2$ kg/m^3; the coefficient of viscosity $\mu = 1.82 \times 10^{-5}$ Ns/m^2; the volume elasticity $E_0 = 1.4 \times 10^5$ Pa; and the speed of sound $c = 340$ m/s. The excitation surface was on top of the main cavity.

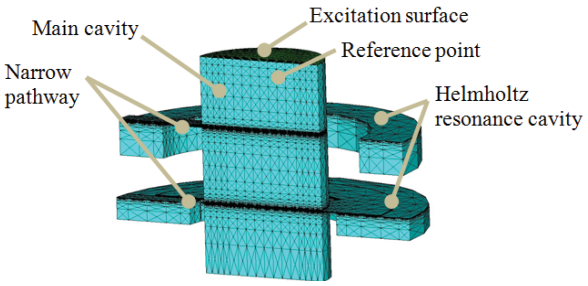

Fig. 4 The ear simulator model for the FEM

The reference point was set to be near the excitation surface,

to simulate a measurement microphone. For the boundary conditions, both ends of the main cavity were defined to be closed, and the particle displacements of all nodes on the outside in contact with the surfaces were fixed, with the exception of nodes on the symmetry plane.

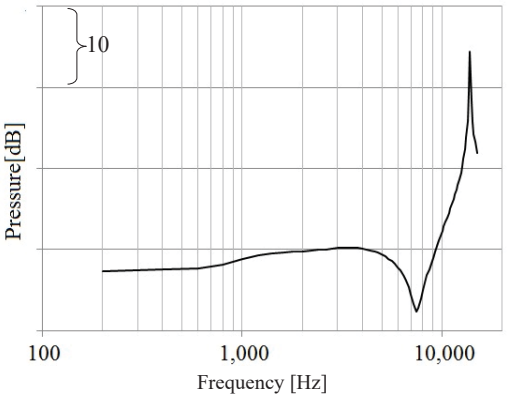

Fig. 5 Pressure vs. frequency

B. FEM Analysis of a Human 3D Ear Canal Model

The frequency response of a 3D human ear canal, as shown in Fig. 6, was modeled using the proposed FEM. Reference points were chosen at three places, since deducing the correct microphone position is difficult in the case of a human ear. Setting the measuring points, slightly apart, helps in reducing the effects of the excitation surface and leakage due to the deformed earplug shape. We used an insert-type earphone. The excitation plane was assumed to be in the center of the earphone sound duct. The excitation plane diameter was approximately 6 mm.

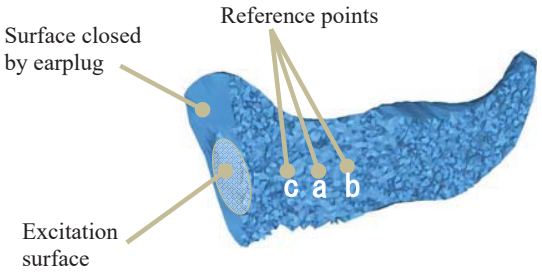

Fig. 6 The 3D human ear canal model and reference points

Fig. 7 shows the frequency response of pressure obtained using FEM. We see that at lower frequencies, there is a significant difference in the modeled pressure at the different measurement points; however, at middle to higher frequencies the calculated pressures follow broadly similar trends. The magnitude of the pressure slightly increases from several hundred hertz to ~2 kHz, reduces once around 2–4 kHz, and then proceeds to increase to a peak in the region of 7–9 kHz.

The numerous peaks and troughs detected in the analysis seem to be caused by resonance phenomena of the tube and Helmholtz resonance phenomena from the effects of the ear canal shape. Since the analysis does not consider the flexibility of the skin and the tympanic membrane, some of the peaks and troughs are predicted to differ from actual measurement results.

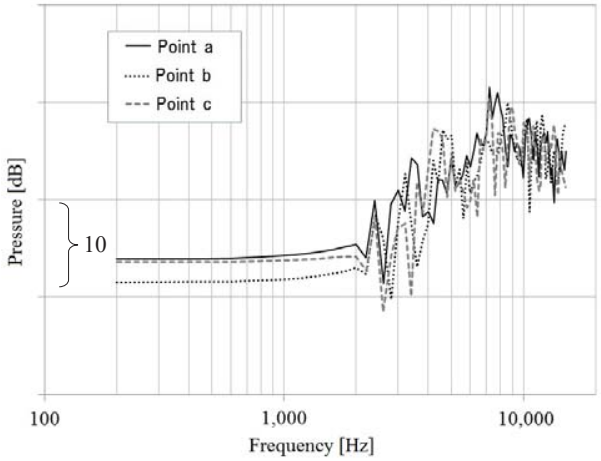

Fig. 7 Pressure vs. frequency at different measurement points, from FEM analysis of a human 3D ear canal model

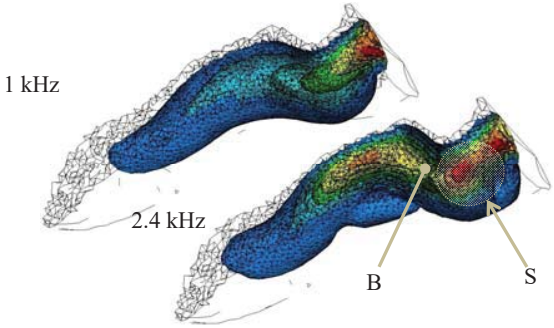

Fig. 8 Displacement distributions at different frequencies

Fig. 8 shows the iso-surface views of particle displacement distributions of the ear canal. Red is used to indicate a large displacement, whereas blue indicates a small displacement. As can be seen, the effect of the shape is small at the lower frequency. However, the effect becomes larger at the higher frequency. For example, in the 2.4 kHz case of this figure, the ear canal has a narrow bending section, *B*. The adjacent space ***S*** becomes a resonator, and seems to have caused resonance phenomena.

Fig. 9 shows the 3D solid mesh model of a human ear as modeled using FEM, with contours showing the calculated element pressure of the model near the resonance conditions. These exhibit a characteristic distribution. Solid color is used to indicate higher pressures, whereas the lack of color indicates a low pressure. This model utilizes the actual CT data of a Japanese adult male, with an overall ear canal length of approximately 29 mm, and a diameter around the measurement points of approximately 8 mm. The FEM uses 99,210 elements and 18,358 nodes. For the analysis, we assumed that nodes in contact with the ear canal (all the surface nodes of this model except the excitation surface) were fixed in position, including the eardrum. The flexibility and displacement of the eardrum is not modeled. Therefore, energy losses due to the vibration of

the eardrum and the flexibility of the skin are not considered. The surface around the excitation surface is assumed to be closed by an earplug. Thus, all nodes on the closed surface were constrained in the xyz directions. We again assumed the effective density, $\rho_0 = 1.2$ kg/m^3; the coefficient of viscosity, $\mu = 1.82 \times 10^{-5}$ Ns/m^2; the volume elasticity, $E_0 = 1.4 \times 10^5$ Pa. From these contours, So-called resonance of tube of length direction tube has occurred. In addition, depending on the ear canal shape and the reflection conditions, it can be deduced that Helmholtz resonance occurs.

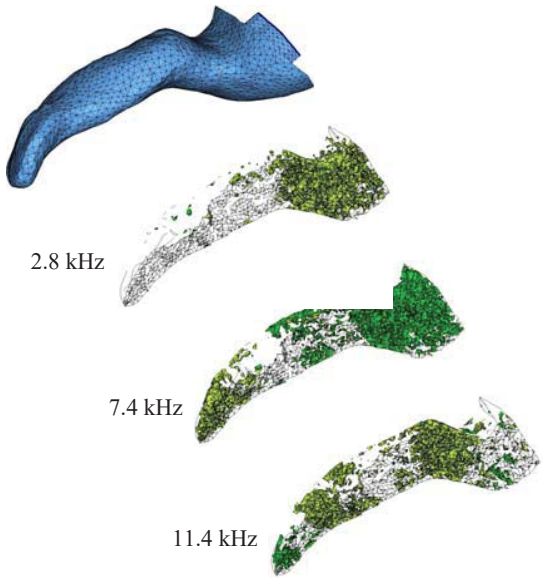

Fig. 9 Pressure distribution at different frequencies, from FEM analysis of a human 3D ear canal model

C. Measurement of Natural Human Ears

To verify the results of the proposed FEM, we measured real human ear data from 18 subjects, of which there were 13 males, and five females. The measurement system, as shown Fig. 10, utilized an FFT analyzer (OROS OR34J-4 4ch Multi-JOB), a microphone (G.R.A.S. type 40BP), a microphone amplifier (G.R.A.S. 14AA Electrostatic Actuator Amplifier) and an ECM (Diameter 3 mm, -44 dB, 2.0 V, 2.2 kΩ). White noise was utilized for the excitation signal, whilst 500 measurements were averaged to produce each data point. The entrance of the ear canal was sealed with an earplug, as shown in Fig. 11.

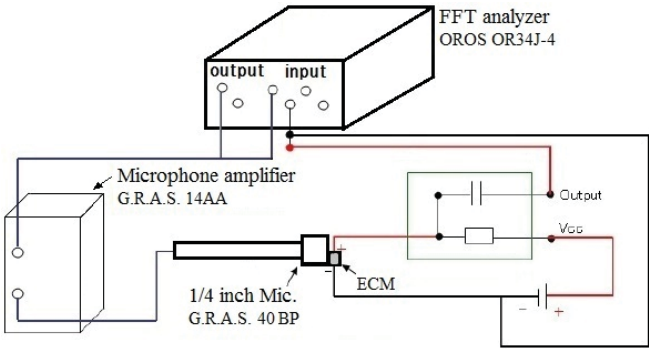

Fig. 10 Equipment setup to measure the frequency response

Fig. 12 shows the averaged measurement results of the 18 test subjects, together with the data from an individual. The magnitude of the pressure slightly increases from several hundred hertz to ~2 kHz, reduces to a minimum around 2 kHz – 5 kHz, and then proceeds to increase to a peak in the region of 7 kHz – 9 kHz.

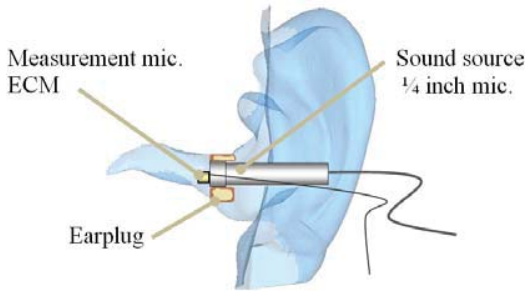

Fig. 11 Microphone setup to measure the frequency response

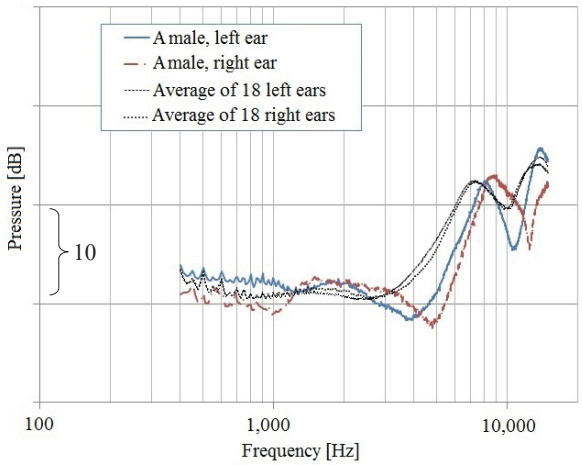

Fig. 12 Measured pressure vs. frequency of 18 human ears

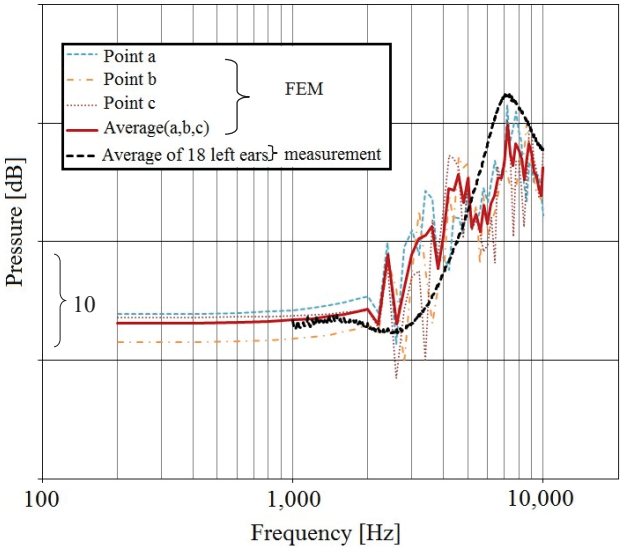

Fig. 13 Comparison of FEM results and measurement data

D. Verification and Comparison of Proposed Method

We analyzed the frequency response of a 3D human ear model using the proposed FEM. Fig. 13 shows the analysis results obtained using the FEM together with measurement data from actual human ears. The FEM data shows sharp peaks and troughs, which we assume to be due to our model ignoring the flexibility of the eardrum. However, the FEM analysis results and the measurement data closely follow a similar trend over the frequency range.

IV. Conclusion

In this paper, we proposed a new acoustic FEM that considers the effects of air viscosity. We used 3D finite element analysis to model both an occluded-ear simulator for insert-type earphones and a 3D solid human ear canal model made from human computed tomography images. We then compared the modeled results with measurements from human ears, showing that the proposed acoustic FEM exhibits good analytical accuracy. We propose to improve our model by investigating the eardrum, since the FEM data showed sharp peaks and troughs that did not match the measured data. We assume this to be due to our model ignoring the flexibility of the eardrum. In addition, in the analysis of the international standard occluded-ear simulator, although the overall trend is similar, the characteristic peaks and troughs shifted to a higher frequency region. This type of ear simulator permits the use of extension tubes. However, since we did not use the extension tube in our model, the overall length was shorter than the typical human ear canal. We propose a further improvement to the model, by including extension tubes. Our next study will incorporate both these improvements and compare the analysis results with measured data.

References

[1] IEC60318-4, IEC standard, Simulators of human head and ear - Part 4: Occluded-ear simulator for the measurement of earphones coupled to the ear by means of ear inserts 2010.

[2] M. Sasajima, T. Yamaguchi, and A. Hara, "Acoustic Analysis Using Finite Element Method Considering Effects of Damping Caused by Air Viscosity in Audio Equipment," *Applied Mechanics and Materials*, vol. 36, pp. 282–286, 2010.

[3] M. Sasajima, T. Yamaguchi, M. Watanabe, Y. Koike, "FEM Analysis of Occluded Ear Simulator with Narrow Slit Pathway," *International Journal of Mechanical, Aerospace, Industrial, Mechatronic and Manufacturing Engineering* vol. 9, No.9, pp. 1430-1433, 2015.

[4] M. A. Biot, "Theory of propagation of elastic waves in a fluid-saturated porous solid. I. Low-frequency range," *Journal of Acoustical Society of America*, vol. 28, pp. 168–178, 1956.

[5] M. A. Biot, "Theory of propagation of elastic waves in a fluid-saturated porous solid. II. Higher-frequency range," *Journal of Acoustical Society of America*, vol. 28, pp. 179–191, 1956.

[6] T. Yamaguchi, "Approximated calculation to damping properties of a closed sound field involving porous materials(proposal of a fast calculation procedure for model damping and damped response)," *Transactions of the Japan Society of Mechanical Engineers, Series C*, vol. 66, no. 648, pp. 2563–2569, 2000.

[7] T. Yamaguchi, H. Nakamoto, Y. Kurosawa, and S. Matsumura "Finite element analysis for damping properties of sound-proof structures having solid body, porous media and air," *Transactions of the Japan Society of Mechanical Engineers, Series A*, vol. 69, no. 677, pp. 34–41, 2003.

[8] T. Yamaguchi, J. Tsugawa, H. Enomoto, and Y. Kurosawa, "Layout of Sound Absorbing Materials in 3D Rooms Using Damping Contributions with Eigenvectors as Weight Coefficients," *Journal of System Design and Dynamics*, vol. 4-1, pp. 166–176, 2010.

[9] T. Yamaguchi, Y. Kurosawa, and H. Enomoto, "Damped Vibration Analysis Using Finite Element Method with Approximated Modal Damping for Automotive Double Walls with a Porous Material," *Journal of Sound and Vibration*, vol. 325, pp. 436–450, 2009.